Adaptive sliding mode and twisting control of a grid-connected spar-buoy floating wind turbine

Orji Williams Ukaegbu, Mohamed Assaad Hamida, Franck Plestan

Adaptive sliding mode and twisting control of a grid-connected spar-buoy floating wind turbine*

Williams Ukaegbu Orji
Nantes Université
École Centrale Nantes
CNRS, LS2N, UMR 6004
F-4400 Nantes, France.
orjiwu@yahoo.com
https://orcid.org/0000-0002-2309-7488

Mohamed Assaad Hamida
Nantes Université
École Centrale Nantes
CNRS, LS2N, UMR 6004
F-4400 Nantes, France.
mohamed.hamida@ec-nantes.fr
https://orcid.org/0000-0003-3682-2463

Franck Plestan
Nantes Université
École Centrale Nantes
CNRS, LS2N, UMR 6004
F-4400 Nantes, France.
franck.plestan@ec-nantes.fr
https://orcid.org/0000-0001-8971-5106

***Abstract*—The floating wind turbines equipped with permanent magnet synchronous generators are complex nonlinear physical systems with multiple degrees of freedom. However, the complexity of these systems, the presence of unmodeled dynamics, and external disturbances pose challenges in maximizing power extraction during low-wind periods. This paper focuses on addressing this challenge for a grid-connected spar-buoy type floating offshore wind turbine (FOWT) operating in Region II. We evaluate the performance of the adaptive sliding mode control and the twisting algorithm to maximize power extraction in the low-wind region and deliver generated electricity to the grid considering the dynamic models of these systems. The controllers' performance is compared against the existing simplified adaptive super-twisting algorithm under identical operating conditions of the FOWT. The co-simulation of the National Renewable Energy Laboratory (NREL) FAST software and the MATLAB/Simulink demonstrate the robustness of the proposed controllers across different conditions regardless of disturbance inputs.**

***Index Terms*—Nonlinear robust control, co-simulation, FOWT, permanent magnet synchronous generator, grid connection.**

I. Introduction

Floating wind turbines offer several economic advantages over fixed-bottom offshore wind turbines, which are typically installed using monopiles anchored to the seabed in water less than 20 meters deep and unlocking new opportunities for offshore wind power. These advantages include economies of scale, faster turnaround on investment, and reduced aesthetic impacts, as discussed in studies such as [1]. Various floating foundation technologies, each with its merits and demerits, are illustrated in Fig. 1 of [2]. These technologies are deployed to harness significant wind energy in offshore areas characterized by water depths exceeding 60 meters, as noted in [2]. Platform movements of the spar-buoy type wind turbine shown in Fig. 4 of [3] engender six degrees of freedom motion, facilitated by a multi-physics-based integration of aerodynamics, electrical control systems for grid connection, hydrodynamics, and the dynamics of mooring lines. These movements are caused by wind speed, wave, and current in the offshore sites.

Over the years, various linear control algorithms have been developed to address uncertainties in offshore wind systems. Some of these controllers, such as the linear quadratic regulator, linear parameter varying, gain scheduling proportional integral, model predictive control, and feed-forward control [4]–[7] have been utilized to optimize FOWT operations. However, these linear control algorithms require extensive tuning effort to compensate for perturbations with unknown bounds during the operation of spar-buoy floating wind turbines.

Furthermore, the back-stepping control [8] has been employed for maximum power point tracking (MPPT) by tip-speed-ratio in low-wind regions. It entails a more complex analysis and exhibits significantly high tracking errors that may compromise maximum power point tracking, primarily due to its dependence on the system model, [8]. Therefore, there is a need to explore nonlinear control strategies that can dynamically enhance power generation during low-wind conditions, ultimately contributing to a more favorable levelized cost of electricity from spar-buoy wind turbines.

This paper presents and evaluates adaptive sliding mode control and the twisting algorithm for maximizing power generation by the FOWT generator and facilitating seamless grid connection within a low-wind region, commonly referred to as Region II. The aerodynamic power piece-wise equation (1) delineates the operation of offshore wind turbines into four distinct regions based on wind speed, as referenced in [5], [7], [8]. It is formulated as follows

$$P_{\text{a}} = \begin{cases} 0, & V < V_{\text{cut-in}} \\ \frac{1}{8}\rho\pi D^2 \eta_{\text{p}}(\lambda,\beta) V^3, & V_{\text{cut-in}} \leq V < V_{\text{rated}} \\ P_{\text{rated}}, & V_{\text{rated}} \leq V < V_{\text{cut-out}} \\ 0, & V_{\text{cut-out}} \leq V. \end{cases} \tag{1}$$

Here, P_{a} and P_{rated} represent the operational and nameplate aerodynamic power in Watts respectively, D denotes the blade diameter in meters, ρ signifies the air density in kgm^{-3}, β is the blade pitch angle in radian, V is the wind speed in ms^{-1}, $\lambda = \frac{\omega_{\text{r}} R}{V}$ and $\eta_{\text{p}}(\lambda,\beta)$ stand for the dimensionless tip-speed-ratio and power coefficient respectively, R is turbine radius.

This paper addresses Region II where the wind speed is within the range of the cut-in $V_{\text{cut-in}}$ $(4.5ms^{-1})$, and below the rated values V_{rated} $(11.4ms^{-1})$, [9]. In Region III, research activity focuses on wind speeds within $V_{\text{rated}} \leq V < V_{\text{cut-out}}(25ms^{-1})$ for power regulation and to reduce the platform oscillation, [3]. Conversely, Region IV lacks enough

literature, but [10] suggested online and offline active load reduction control methods for wind speeds above the cut-out value.

II. Model of the system

A. Spar-buoy type FOWT

The main physical components considered in the dynamic models of the 5MW OC3 Hywind spar-buoy and grid systems in this study includes the drive train system, the FOWT generator, and the grid subsystems [4], [9], [11], [12]. The floating wind turbine linearized model operated within Region II [13] is written as

$$\dot{x} = Ax + B_{\tau_{\mathrm{g}}}\tau_{\mathrm{g}} + B_{\beta}(\beta_{0})\dot{\beta} + B_{\mathrm{d}}d_{0} \tag{2}$$

$$x = [\ \phi \quad \dot{\phi} \quad \omega_{r}\ ]^{T} \tag{3}$$

where d_0 is the disturbance input to the system, the platform pitch and the pitch rate are ϕ and $\dot{\phi}$ respectively, β_{0} is a constant reference blade pitch angle, such that $\dot{\beta} = 0$, and the generator torque τ_{g} is required to be maximum to achieve the control objective. Definitions of the matrices A, B_{d} and the constant coefficient $B_{\tau_{\mathrm{g}}}$ are detailed in [13]. If all the states are available and measurable, system (2) can be rewritten in the form

$$\dot{x} = f(x) + g(x)\cdot \upsilon \tag{4}$$

where $f(x) = Ax + B_{\mathrm{d}}d_{0}$ with the disturbance input d_0, and $g(x)\cdot\upsilon = B_{\tau_{\mathrm{g}}}\tau_{\mathrm{g}}$, the generator torque being the control input, designed via the generator q-axis stator current subset. Both $f(x)$ and $g(x)$ contain uncertain functions, hence it is imperative to design a robust control that will guarantee maximum generator torque. The dynamic models of both the generator and the grid are elaborated in the subsequent section.

B. Generator model

The FOWT generator and the drive train models are represented from [13], [14] for power maximizing power extraction in Region II with wind speed $V_{\text{cut-in}} \le V < V_{\text{rated}}$

$$\underbrace{\begin{bmatrix}\dot{i}_{d}\\ \dot{i}_{q}\\ \dot{\omega}_{\mathrm{g}}\end{bmatrix}}_{\dot{\bar{x}}} = \underbrace{\begin{bmatrix}-\frac{R_{s}}{L_{d}}i_{d} + p\frac{L_{q}}{L_{d}}\omega_{\mathrm{g}}i_{q}\\ -\frac{R_{s}}{L_{q}}i_{q} - p\frac{L_{d}}{L_{q}}\omega_{\mathrm{g}}i_{d} - p\frac{1}{L_{q}}\phi_{f}\omega_{\mathrm{g}}\\ \frac{N_{\mathrm{g}}(\tau_{a} - N_{\mathrm{g}}\tau_{g})}{J}\end{bmatrix}}_{f(\bar{x})} + \underbrace{\begin{bmatrix}\frac{1}{L_{d}} & 0\\ 0 & \frac{1}{L_{q}}\\ 0 & 0\end{bmatrix}}_{g(\bar{x})}\cdot\underbrace{\begin{bmatrix}v_{d}\\ v_{q}\end{bmatrix}}_{\bar{v}} \tag{5}$$

$$\tau_{\mathrm{g}} = \begin{cases}\frac{3}{2}p\left(L_{d} - L_{q}\right)i_{d}i_{q} + \frac{3}{2}p\phi_{f}i_{q}, & \text{if } L_{d} \neq L_{q}\\ \frac{3}{2}p\phi_{f}i_{q}, & \text{if } L_{d} = L_{q}\end{cases} \tag{6}$$

where R_s represents the generator resistance (Ω), i_d and i_q denote the dq stator currents (A), p indicates the number of pole pairs, L_d and L_q are the dq axis inductance (H), ϕ_f signifies the magnetic flux (Wb), $\bar{v} = [v_d \quad v_q]^T$ stand for the generator dq control inputs voltage (V) vector, N_g represents the gearbox ratio, $\omega_{\mathrm{g}} = \frac{30N_{g}\omega_{\mathrm{r}}}{\pi}$ (RPM) denotes the generator speed, and $\tau_{\mathrm{a}} = \frac{P_{\mathrm{a}}}{\omega_{\mathrm{r}}}$ represents the aerodynamic torque (Nm). When considering a surface mount PMSG, the generator inductance $L_{d} = L_{q}$. Incorporating a loss term P_{loss}, the generator active power P_e and the reactive Q_e power are expressed as $P_{e} = \frac{3}{2}\left(v_{q}i_{q} + v_{d}i_{d} - \frac{2}{3}P_{loss}\right)$, $Q_{\mathrm{e}} = \frac{3}{2}\left(v_{q}i_{d} - v_{d}i_{q} - \frac{2}{3}P_{loss}\right)$ and $P_{loss} = \frac{3}{2}R_{s}\left(i_{d}^{2} + i_{q}^{2}\right)$. The generated active power is transmitted to the grid for further distribution to substations and load centers. Details of nominal values of the generator parameters are in the study [3]. We consider the grid model [11], [12] in the sequel.

C. Grid model

The grid model when the voltage vector is oriented in the q-xis, and neglecting the converter losses is represented from [11]

$$\underbrace{\begin{bmatrix}\dot{i}_{gd}\\ \dot{i}_{gq}\\ \dot{v}_{dc}\end{bmatrix}}_{\dot{\tilde{x}}} = \underbrace{\begin{bmatrix}\frac{-R_{g}i_{gd}}{L_{g}} + \omega i_{gq} - \frac{\Psi_{d}}{L_{g}}\\ \frac{-R_{g}i_{gq}}{L_{g}} - \omega i_{gd} - \frac{\Psi_{q}}{L_{g}}\\ \frac{P_{e}}{Cv_{dc}} - \frac{P_{\mathrm{g}}}{Cv_{dc}}\end{bmatrix}}_{f(\tilde{x})} + \underbrace{\begin{bmatrix}\frac{1}{L_{g}} & 0\\ 0 & \frac{1}{L_{g}}\\ 0 & 0\end{bmatrix}}_{g(\tilde{x})}\cdot\underbrace{\begin{bmatrix}v_{gd}\\ v_{gq}\end{bmatrix}}_{\tilde{v}} \tag{7}$$

with $P_{\mathrm{g}} = \frac{3}{2}v_{gq}i_{gq}$ and $Q_{\mathrm{g}} = \frac{3}{2}v_{gq}i_{gd}$; where i_{qd}, i_{gq} represent the grid dq axis currents (A), $\tilde{v} = [v_{gd} \quad v_{gq}]^{T}$ denote the grid dq-axis control inputs voltage (V) vector, respectively. R_g stands for the converter resistance (R), Ψ_d, Ψ_q represent the grid dq axis root-mean-square voltage (V), L_g signifies the inductance of the grid-side converter (H), and $\omega = 2\pi f_{g}$ denotes the grid angular frequency. v_{dc} denotes the DC link voltage, C represents the capacitance (F) storing power flowing in and out of the DC link, P_{g} and Q_{g} are the grid active and reactive power, respectively. The value of the DC link reference parameter is from [11] and the nominal values are shown in the sequel.

III. Control objectives

The control objective is to maximize power production in Region II regardless of external disturbances while ensuring a stable floating platform. To achieve the control objectives, the control system focuses on optimizing the generator q-axis current i_{q}, and its reference value i_{q0} is chosen as a function of the generator speed, allowing for dynamic adjustment of the current, a function of the electromagnetic torque, to maximize power extraction. Furthermore, a small constant reference blade pitch angle of $\beta_0 = 0.04$ radian [13] at an optimum efficiency of $\eta_p = 0.48$ [9] is maintained to stabilize the wind turbine operation in Region II.

Generator current references

The control is designed such that the stator currents i_d and i_q track their references i_{d0} and i_{q0}, respectively defined as $i_{\mathrm{d0}} = 0$ [14] and $i_{\mathrm{q0}} = \frac{2P_{0}}{3p\phi_{f}N_{g}\omega_{\mathrm{r}}}$ [11], where P_0 in this study is the spar-buoy wind turbine rated power related to the partial load of low wind region. This choice of reference guarantees maximum power tracking point by maximum torque. The d-axis current reference $i_{\mathrm{d0}} = 0$, aiming to minimize the drive

train oscillation [3], [14], thereby contributing to the overall performance and reliability of the wind turbine.

Grid references

The objective of the direct current subsystem is to ensure a constant grid voltage, as required by the grid code standards discussed in [11]. This is achieved by controlling the DC link voltage v_{dc} to track a constant reference v_{dc0} as in [11]. The DC link provides its virtual input i_{gq0} as a reference to the grid q-axis current i_{gq}, and the grid d-axis current i_{gd} is controlled to track its reference $i_{\text{gd0}} = 0$; while the grid voltage vector is oriented in the q-axis to guarantee maximum active power.

IV. Control design

The dynamic system given by (4) is nonlinear, described as

$$\begin{aligned} \dot{x} &= f(x) + g(x) \cdot \upsilon \\ y &= h(x). \end{aligned} \tag{8}$$

Here, the terms $f(x)$ and $g(x)$ represent bounded and unknown nonlinear functions of the state x, υ denotes the control input, and y signifies the system output. The sliding variable $S = S(x,t)$ is defined such that when $S = 0$, the system output converges to zero. A first-order sliding mode occurs when $S = 0$, and a second-order sliding mode occurs when $S = \dot{S} = 0$ in finite as discussed in [3], [15], [16] regardless of the disturbance inputs, if certain conditions which are shown subsequently are satisfied.

Assumption I

The sliding variable $S(x,t)$ is defined with respect to the system output y and assumes a relative degree of unity. Then, we suppose that S-dynamics reads as [16]

$$\dot{S} = \Gamma(x,t) + \xi(x,t)\upsilon \tag{9}$$

where $\Gamma(x,t)$ and $\xi(x,t)$ are unknown and bounded functions such that $|\Gamma| \leq \Gamma_{_M}, \quad 0 < \xi_m \leq \xi \leq \xi_{_M}$ and $\xi(x,t) \neq 0$ for all $x \in X \ t > 0$, with Γ_M, ξ_m and ξ_M being positive constants.

Assumption II

The S-dynamics expressed as

$$\dot{S} = \underbrace{\frac{\partial S}{\partial t} + \frac{\partial S}{\partial x} f(x,t)}_{\Gamma(x,t)} + \underbrace{\frac{\partial S}{\partial x} g(x,t)}_{\xi(x,t)} \cdot \upsilon \tag{10}$$

$$\Gamma(x,t) = \Gamma_0(\cdot) + \Gamma_u(\cdot) \tag{11}$$

$$\xi(x,t) = \xi_0(\cdot) + \xi_u(\cdot) \tag{12}$$

with Γ_0 and ξ_0 representing known functions, while Γ_u and ξ_u denote unknown and bounded uncertainties, respectively. In the case of the spar buoy-type FOWT subject to uncertainties and perturbations from various sources, including structural elasticity in towers, blades, environmental factors, and parameter variation are represented in the functions $f(x,t)$ and $g(x,t)$. Despite these disturbances, the control objective is to design υ that ensures that S-dynamic in (12) is forced to a vicinity of 0. The linearized state feedback for the S-dynamics is given by

$$\upsilon = \frac{1}{\xi_0}\left(-\Gamma_0(\cdot) + u\right). \tag{13}$$

In the sequel, the first-order and second-order sliding mode control [3], [15] respectively, will be applied to u to guarantee robustness and finite time convergence of the system states regardless of the disturbance inputs.

A. Robust controllers

Super-twisting algorithm [15]

The super-twisting algorithm (STW) for control is defined as

$$\begin{aligned} u &= -\gamma_{_1}|S|^{\frac{1}{2}} \cdot sign(S) + \Phi \\ \dot{\Phi} &= -\gamma_2 \cdot sign(S). \end{aligned} \tag{14}$$

Here, u represents the STW control input, subject to the following sufficient conditions: $\gamma_{_1} > \frac{\Gamma_M}{\xi_M}$ and $\gamma_2^2 \geq \frac{4\Gamma_M \cdot \xi_M}{\xi_m^3} \cdot \frac{\gamma_1 + \Gamma_M}{\gamma_1 - \Gamma_M}$, which ensures $S = \dot{S} = 0$. The use of fixed gains in the STW significantly reduces high-frequency chattering, a common issue in first-order sliding mode control, as noted by [16] by its continuous control function, ensuring the convergence of the sliding variable to the sliding surface within a finite time, regardless of perturbations. The challenge remains in determining the bounds of perturbations, necessitating significant control efforts.

Simplified adaptive super-twisting SAST [17]

To address the aforementioned challenges, the gains $\gamma_{_1}$ and γ_2 in the STW algorithm (14) are dynamically adjusted online to counteract disturbances and minimize tuning effort as detailed in [3], with $\gamma_{_1} = -2L$ and $\gamma_{_2} = -\frac{L^2}{2}$. L is adapted online as

$$\dot{L} = \begin{cases} L(|S| - \mu), & \text{if } L > L_{\text{m}} \\ L_m, & \text{if } L \leq L_{\text{m}}. \end{cases} \tag{15}$$

Here, μ and L_m are small positive constants, with the μ contributing to the accuracy of the system. Studies in [3], [15], [16] utilize second-order super-twisting algorithm to demonstrate the stability criterion.

Twisting control [15]

The twisting control (TWT) is a discontinuous controller suitable for systems with a relative degree of unity to the sliding variable, as discussed in [16]. The algorithm is defined as (16). Details regarding the stability conditions of the positive constants ζ_1 and ζ_2 can be found in the study by [15], [16]

$$u = -\zeta_1 sign(S) - \zeta_2 sign(\dot{S}). \tag{16}$$

Sliding mode control [16]

The sliding mode control (SMC) is well known for its insensitivity to bounded perturbations and finite time convergence of complex dynamic systems such as the spar-buoy type FOWT. The sliding mode control [16] is formulated as

$$u = -Ksign(S). \tag{17}$$

K being the control gain ensuring $S = 0$ in finite time if the condition $K \geq \frac{\Gamma_M + \eta}{\xi_m}$ is satisfied. The η-attractive condition validates a strict requirement for finite time convergence of the sliding variable S towards the origin, $S\dot{S} \leq -\eta|S|$, with $\eta > 0$, [16]. However, the first-order sliding mode control has limitations due to chattering challenges engendered by high-frequency switching functions, potentially affecting system performance efficiency. To address this, the second-order sliding mode control, which depends on the sliding variable S and reduces the chattering effect was introduced.

Adaptive sliding mode control ASMC [18]

The adaptive gain for the sliding mode control (17) of nonlinear systems with disturbances of unknown bounds, ensuring finite time convergence without over-estimation of gains, are developed in studies by [18]. The adaptive SMC reads

$$\dot{K} = \begin{cases} \bar{K}|S|sign(|S| - \hat{\mu}), & \text{if } K > \epsilon \\ \\ \epsilon, & \text{if } K \leq \epsilon \end{cases} \tag{18}$$

where $\bar{K}$, ϵ and $\hat{\mu}$ are small positive constants with $\hat{\mu}$ being responsible for accuracy of the system.

The gain scheduling PI [5] reference controller is used to compare results obtained from the proposed controllers.

B. Generator control design

The generator q-axis stator current sliding variable

$$\begin{aligned} S_{\mathrm{q}} &= i_q - i_{\mathrm{q0}} \\ \dot{S}_{\mathrm{q}} &= \dot{i}_q - \dot{i}_{\mathrm{q0}} \end{aligned} \tag{19}$$

$$\underbrace{\dot{S}_{\mathrm{q}}}_{\dot{S}_q} = \underbrace{-\frac{R_s}{L_q} i_q - p\frac{L_d}{L_q}\omega_{\mathrm{g}} i_d - p\frac{\phi_f}{L_q}\omega_{\mathrm{g}} - \dot{i}_{\mathrm{q0}}}_{\Gamma_q(x,t)} + \underbrace{\frac{1}{L_q}}_{\xi_q(x,t)} v_q \tag{20}$$

where $\Gamma_q(x,t) = \Gamma_{q0} + \Gamma_{qu}$, $\xi_q(x,t) = \xi_{q0} + \xi_{qu}$ as previously detailed in (9)-(13). This implies the resistor $R_s = R_{s0} + R_{su}$, the inductors $L_d = L_{d0} + L_{du}$, $L_q = L_{q0} + L_{qu}$ and the magnetic flux $\phi_f = \phi_{f0} + \phi_{fu}$. R_{s0}, L_{d0}, ϕ_{f0} and L_{q0} representing the nominal values provided by the nameplate of the wind turbine is gotten from [3]. R_{su}, ϕ_{fu}, L_{du} and L_{qu} denote the uncertainties of the generator parameters. The sliding variable S_q has a relative degree of unity with respect to v_q and its S_q-dynamic is written as in (20). The generator q-axis control input v_q that forces the sliding variable $S_q \to 0$ is expressed as in (21)

$$\begin{aligned} v_q &= \frac{1}{\xi_{q0}} \left(-\Gamma_{q0}(\cdot) + u_q\right) \\ v_q &= R_{s0} i_q + pL_{d0}\omega_{\mathrm{g}} i_d + p\phi_{f0}\omega_{\mathrm{g}} + L_{q0}\dot{i}_{\mathrm{q0}} + L_{q0} u_q. \end{aligned} \tag{21}$$

where u_q denotes the q-axis robust control law.

C. Grid control design

Direct current link control

The direct current sliding variable

$$\begin{aligned} S_{\mathrm{dc}} &= v_{dc} - v_{dc0} \\ \dot{S}_{\mathrm{dc}} &= \dot{v}_{dc} - \dot{v}_{dc0} \end{aligned} \tag{22}$$

$$\underbrace{\dot{S}_{\mathrm{dc}}}_{\dot{S}_{\mathrm{dc}}} = \underbrace{\frac{P_e}{Cv_{dc}} - \dot{v}_{dc0}}_{\Gamma_{dc}(x,t)} - \underbrace{\frac{3}{2}\frac{v_{gq}}{Cv_{dc}}}_{\xi_{dc}(x,t)} i_{gq}. \tag{23}$$

where $\Gamma_{dc}(x,t) = \Gamma_{dc0} + \Gamma_{dcu}$ and $\xi_{dc}(x,t) = \xi_{dc0} + \xi_{dcu}$ as detailed in (9)-(13) implying the capacitor $C = C_0 + C_u$; with C_0 and C_u being the nominal and uncertain parts respectively. If $i_{\mathrm{gq}} = i_{\mathrm{gq0}}$ is set to design a virtual input for the direct current link, which is subsequently used as the grid q-axis reference and the relative degree of S_{dc} with respect to i_{gq0} is 1. Then, the S_{dc}-dynamic is defined as in (23). The DC link virtual input i_{gq0} which forces $S_{\mathrm{dc}} \to 0$ is written as

$$\begin{aligned} i_{\mathrm{gq0}} &= \frac{1}{\xi_{dc0}} \left(-\Gamma_{dc0}(\cdot) + u_{dc}\right) \\ i_{\mathrm{gq0}} &= \frac{2}{3}\frac{P_e}{v_{gq}} - \frac{2}{3}\frac{C_0 v_{dc}\dot{v}_{dc0}}{v_{gq}} - \frac{2}{3}\frac{C_0 v_{dc}}{v_{gq}} u_{dc} \end{aligned} \tag{24}$$

The u_{dc} denotes the DC link robust control law. It is noteworthy that a negative coefficient appears in the DC link control law, implying a virtual inner loop that ensures i_{gq0} serves as a reference for the grid q-axis current i_{gq}. This approach contrasts with existing procedures detailed in (9)-(13). At the direct current subsystem, the relationship $v_{dc} i_{\mathrm{dc}} = v_{\mathrm{gq}} i_{\mathrm{gq}}$ holds [12], where i_{dc} is the DC link direct current in amperes.

Grid current control

The sliding variable of the grid q-xis is written as

$$\begin{aligned} S_{\mathrm{gq}} &= i_{\mathrm{gq}} - i_{\mathrm{gq0}} \\ \dot{S}_{\mathrm{gq}} &= \dot{i}_{\mathrm{gq}} - \dot{i}_{\mathrm{gq0}} \end{aligned} \tag{25}$$

$$\underbrace{\dot{S}_{\mathrm{gq}}}_{\dot{S}_{gq}} = \underbrace{\frac{-R_g i_{\mathrm{gq}}}{L_g} - \omega i_{gd} - \frac{\Psi_q}{L_g} - \dot{i}_{\mathrm{gq0}}}_{\Gamma_{gq}(x,t)} + \underbrace{\frac{1}{L_g}}_{\xi_{gq}(x,t)} v_{gq}. \tag{26}$$

with $\Gamma_{gq}(x,t) = \Gamma_{gq0} + \Gamma_{gqu}$ and $\xi_{gq}(x,t) = \xi_{gq0} + \xi_{gqu}$ following details in (9)-(13). Hence, $R_g = R_{g0} + R_{gu}$, $L_g = L_{g0} + L_{gu}$. The S_{gq}-dynamic is written in (26) and its relative degree in relation to the control input v_{gq} is 1. The control input v_{gq} which forces $S_{\mathrm{gq}} \to 0$ becomes

$$\begin{aligned} v_{gq} &= \frac{1}{\xi_{gq0}} \left(-\Gamma_{gq0}(\cdot) + u_{gq}\right) \\ v_{gq} &= R_{g0} i_{\mathrm{gq}} + \omega L_{g0} i_{gd} + \Psi_q + L_{g0}\dot{i}_{\mathrm{gq0}} + L_{g0} u_{gq} \end{aligned} \tag{27}$$

u_{gq} denotes the grid q-axis robust control law. The nominal values of the grid parameters are $R_{g0} = 0.0002\,\Omega$, f_g = 60 Hz, $\omega = 377.04\,\mathrm{rad\,s^{-1}}$, $\Psi_q(RMS) = 220\,\mathrm{V}$, $L_{g0} = 0.006\,\mathrm{H}$, $C_0 = 4.15 \times 10^{-4}\,\mathrm{F}$, while L_{gu}, R_{gu} and C_u represent the uncertainties.

V. Simulations and Results

This study features the NREL 5MW OC-3 Hywind spar-buoy type floating offshore wind turbine in the FAST software and MATLAB/Simulink co-simulation. It incorporates 24 degrees of freedom of the FAST software, conducted with a fixed step size of 12.5ms and employs the Euler integration algorithm. To assess the effectiveness of the proposed controllers,

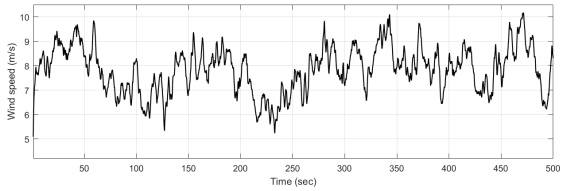

Fig. 1: Wind speed condition (Region II).

they are compared against established control methodologies, specifically the simplified adaptive super-twisting and the gain scheduling proportional integral controllers under identical conditions including an irregular wave with a significant elevation of 1.08 meters and a peak spectral period of 9.7 seconds. A mean stochastic wind speed condition 8 ms^{-1} shown in Fig. 1 and a 15% turbulence intensity characterized perturbations.

The ASMC and the SAST algorithm parameters are tuned $\hat{\mu} = 0.01$, $\epsilon = 0.01$, $\bar{K} = 0.1$ and $\mu = 0.9$, $L_m = 0.0001$ respectively, to get better performance for both the generator and the grid control designs. The fixed-gains twisting, super-twisting and the gain scheduling proportional integral control parameters are $\zeta_1 = 2.5$, $\zeta_2 = 2.5$, $\gamma_1 = 2.5$, $\gamma_2 = 2.4$, $K_P = 2.9$ and $K_I = 2.5$, respectively for the generator side control. The constant gains used for the twisting, super-twisting and the gain scheduling proportional integral grid side control are $\zeta_{1*} = 30$, $\zeta_{2*} = 90$, $\gamma_{1*} = 30$, $\gamma_{2*} = 90$; $K_{P*} = 30$ and $K_{I*} = 92$ respectively, while the FOWT parameter values are obtained from [9]. The following bands $\pm 5\%$ uncertainties is considered for the L_{du}, L_{qu} and ϕ_{fu} respectively, and $\pm 2\%$ is considered for the R_{su}, L_{gu}, R_{gu} and C_u respectively.

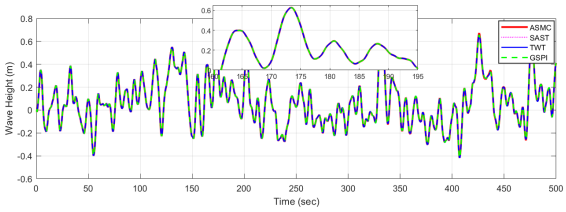

Fig. 2: Wave height.

Figure 2 depicts the wave height evolution of ASMC (red line), SAST(magenta line), TWT(blue line), and the gain scheduling PI(green line), respectively. The normalized Damage Equivalent Loads (DEL) for the FOWT mooring lines forces and the blade root moments are used to compare the controllers in the sequel.

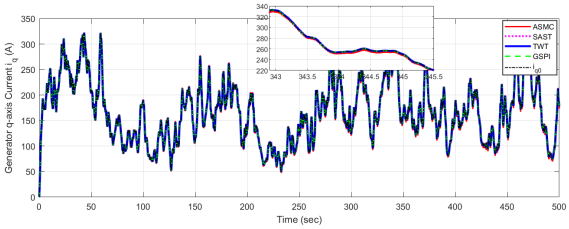

Fig. 3: Comparison of generator current.

A. Generator side control

Figure 3 shows the tracking performance of ASMC(red), SAST(magenta), TWT(blue), and the gain scheduling PI(green) controllers to their reference i_{q0}(black), which guarantees maximum electromagnetic torque. Consequently, maximum power is generated within Region II. The generated power is depicted in Fig. 4 tracking the nameplate reference power P_0 associated with the spar-buoy wind turbine partial load operation.

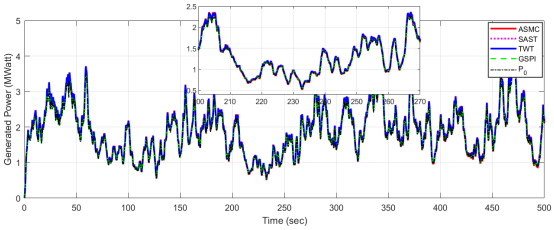

Fig. 4: Comparison of generated power.

B. Grid side control

The DC link control balances the wind turbine generator and the grid power. The control guarantees the DC link voltage control and gives a reference to the grid q-axis current. The grid current q-axis tracks its reference from the DC link. Indeed, the controllers exhibit an efficient energy conversion, facilitating optimal current transfer from the generator-side subsystem to the grid-side subsystem. Hence, the active power of the grid is depicted in Fig. 5 for various controllers.

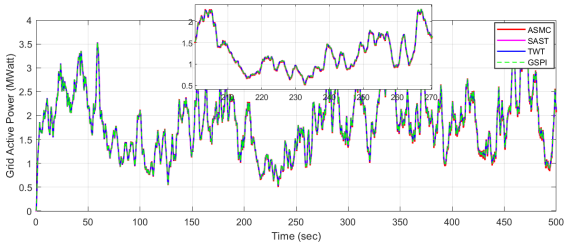

Fig. 5: Comparison of grid active power.

Analysis of Blade Moments

Fig. 6 (top) shows the normalized DEL (Damage Equivalent Loads) for the blade root moments, specifically RootMxb1, RootMyb1, RootMxb2, RootMyb2, RootMxb3, and

RootMyb3. The DEL values are normalized to a reference gain-scheduling PI load, typically set to unity for comparison. All three methods (ASMC(blue), SAST(orange), TWT(yellow)) show very similar normalized DEL values, close to 1, indicating that the differences in blade root moments among these control strategies are minimal.

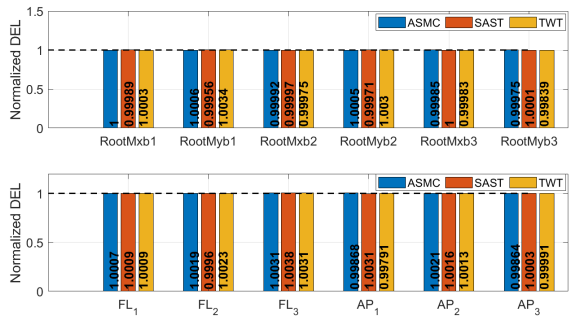

Fig. 6: Normalized structural DEL values: **(Top)** Blade root moments, and **(Bottom)** Mooring lines forces.

Analysis of mooring line tension forces

The fairlead (FAIRTEN) points FL1-FL3 and the anchor (ANCHTEN) points AP1-AP3 shown in Fig. 6 (bottom) represent the mooring lines tension forces on the floating platform and seabed attachments respectively. The controllers exhibit efficient performance hovering within the reference controller. The SAST has improved performance for FL2 compared to ASMC and the fixed gain-twisting controllers.

VI. Conclusion

The proposed controllers were evaluated using the full degree of freedom of the FAST multi-physics software in various scenarios and were compared against simplified adaptive super-twisting and gain scheduling proportional-integral controllers in terms of power maximization and floating platform characteristics. Results from performance indicators and simulations demonstrate the robustness of the controllers across different conditions. Future studies will focus on implementing the proposed controllers in other floating wind turbines with higher nameplate power, such as the DTU 10 MW and IEA 15 MW models, as well as on the OC4 platform [13]. In addition, developing and applying large-eddy simulation techniques [19] to assess dynamics behaviors of wind and waves on a wind farm efficiency is an interest.

Acknowledgement

The research of Williams Ukaegbu Orji was supported by the Petroleum Technology Development Fund (PTDF), a Federal Government Agency of the Federal Republic of Nigeria, on the grant number (1919PHD065). This conference registration is financed by the ANR project CREATIF (ANR-20-CE05-0039) and DENS (101120278), France.

References

[1] A. Otter, J. Murphy, V. Pakrashi, A. Robertson, C. Desmond, A review of modelling techniques for floating offshore wind turbines, Wind Energy 25 (5) (2022) 831–857.
URL https://doi.org/10.1002/we.2701

[2] H. Basbas, Y.-C. Liu, S. Laghrouche, M. Hilairet, F. Plestan, Review on floating offshore wind turbine models for nonlinear control design, Energies 15 (15) (2022) 5477.
URL https://www.mdpi.com/1748766

[3] C. Zhang, A contribution to the nonlinear control of floating wind turbines, Ph.D. thesis, École centrale de Nantes (2021).
URL https://theses.hal.science/tel-03268023/

[4] M. Singh, E. Muljadi, J. Jonkman, V. Gevorgian, I. Girsang, J. Dhupia, Simulation for wind turbine generators–with fast and matlab-simulink modules, Tech. rep., National Renewable Energy Lab.(NREL), Golden, CO (United States) (2014).
URL https://doi.org/10.2172/1130628

[5] O. Bagherieh, R. Nagamune, Gain-scheduling control of a floating offshore wind turbine above-rated wind speed, Control Theory and Technology 13 (2) (2015) 160–172.
URL https://doi.org/10.1007/s11768-015-4152-0

[6] P. Zhao, R. Nagamune, Switching lpv control of a floating offshore wind turbine on a semi-submersible platform, in: 2019 IEEE 28th International Symposium on Industrial Electronics (ISIE), IEEE, 2019, pp. 664–669.
URL https://doi.org/10.1109/ISIE.2019.8781153

[7] D. Schlipf, L. Y. Pao, P. W. Cheng, Comparison of feedforward and model predictive control of wind turbines using lidar, in: 2012 IEEE 51st IEEE Conference on Decision and Control (CDC), IEEE, 2012, pp. 3050–3055.
URL https://doi.org/10.1109/CDC.2012.6426063

[8] E. Aslmostafa, M. A. Hamida, F. Plestan, Nonlinear control strategies for a floating wind turbine with pmsg in region 2: A comparative study based on the openfast platform, Ocean Engineering 300 (2024) 117507.

[9] J. Jonkman, S. Butterfield, W. Musial, G. Scott, Definition of a 5-mw reference wind turbine for offshore system development, Tech. rep., National Renewable Energy Lab.(NREL), Golden, CO (US) (2009).

[10] M. Jelavic, V. Petrovic, M. Barišic, I. Ivanovic, Wind turbine control beyond the cut-out wind speed, in: Annual Conference and Exhibition of European Wind Energy Association (EWEA2013), 2013.

[11] S. Marmouh, M. Boutoubat, L. Mokrani, M. Machmoum, A coordinated control and management strategy of a wind energy conversion system for a universal low-voltage ride-through capability, International Transactions on Electrical Energy Systems 29 (8) (2019) e12035.
URL https://doi.org/10.1002/2050-7038.12035

[12] F. Poitiers, T. Bouaouiche, M. Machmoum, Advanced control of a doubly-fed induction generator for wind energy conversion, Electric Power Systems Research 79 (7) (2009) 1085–1096.
URL https://doi.org/10.1016/j.epsr.2009.01.007

[13] N. Abbas, D. Zalkind, L. Pao, A. Wright, A reference open-source controller for fixed and floating offshore wind turbines, Wind Energy Science Discussions 2021 (2021) 1–33.
URL https://doi.org/10.5194/wes-7-53-2022

[14] F. Plestan, C. Evangelista, P. Puleston, I. Guenoune, Control of a twin wind turbines system without wind velocity information, in: 2018 15th International Workshop on Variable Structure Systems (VSS), IEEE, 2018, pp. 150–155.
URL https://doi.org/10.1109/VSS.2018.8460274

[15] A. Levant, Sliding order and sliding accuracy in sliding mode control, International journal of control 58 (6) (1993) 1247–1263.
URL https://doi.org/10.1080/00207179308923053

[16] Y. Shtessel, C. Edwards, L. Fridman, A. Levant, et al., Sliding mode control and observation, Vol. 10, Springer, 2014.

[17] S. V. Gutierrez, J. De León-Morales, F. Plestan, O. Salas-Peña, A simplified version of adaptive super-twisting control, International Journal of Robust and Nonlinear Control 29 (16) (2019) 5704–5719.

[18] F. Plestan, Y. Shtessel, V. Bregeault, A. Poznyak, New methodologies for adaptive sliding mode control, International journal of control 83 (9) (2010) 1907–1919.
URL https://doi.org/10.1080/00207179.2010.501385

[19] A. Stieren, S. N. Gadde, R. J. Stevens, Modeling dynamic wind direction changes in large eddy simulations of wind farms, Renewable Energy 170 (2021) 1342–1352.